NASA Technical Memorandum 105614

10 kW Power Electronics for Hydrogen Arcjets

John A. Hamley, Luis R. Pinero,
and Gerald M. Hill
Lewis Research Center
Cleveland, Ohio

Prepared for the
1992 JANNAF Propulsion Meeting
Indianapolis, Indiana, February 24–28, 1992

NASA

10 kW POWER ELECTRONICS FOR HYDROGEN ARCJETS

John A. Hamley, Luis R. Pinero, and Gerald M. Hill
National Aeronautics and Space Administration
Lewis Research Center
Cleveland, Ohio 44135

SUMMARY

A combination of emerging mission considerations such as "launch on schedule," resource limitations, and the development of higher power spacecraft busses has resulted in renewed interest in high power hydrogen arcjet systems with specific impulses greater than 1000 s for Earth-space orbit transfer and maneuver applications. Solar electric propulsion systems with about 10 kW of power appear to offer payload benefits at acceptable trip times. This work outlines the design and development of 10 kW hydrogen arcjet power electronics and results of arcjet integration testing. The power electronics incorporated a full bridge switching topology similar to that employed in state of the art 5 kW power electronics, and the output filter included an output current averaging inductor with an integral pulse generation winding for arcjet ignition. Phase shifted, pulse width modulation with current mode control was used to regulate the current delivered to the arcjet, and a low inductance power stage minimized switching transients. Hybrid power Metal Oxide Semiconductor Field Effect Transistors were used to minimize conduction losses. Switching losses were minimized using a fast response, optically isolated, totem-pole gate drive circuit. The input bus voltage for the unit was 150 V, with a maximum output voltage of 225 V. The switching frequency of 20 kHz was a compromise between mass savings and higher efficiency. Power conversion efficiencies in excess of 0.94 were demonstrated, along with steady state load current regulation of 1 percent. The power electronics were successfully integrated with a 10 kW laboratory hydrogen arcjet, and reliable, nondestructive starts and transitions to steady state operation were demonstrated. The estimated specific mass for a flight packaged unit was 2 kg/kW.

INTRODUCTION

During the late 1950's and early 1960's, much work was focused on the development of arcjets for planetary propulsion applications. These efforts were recently summarized by Sankovic et al. (ref. 1). Emphasis was placed on the development of a 30 kW radiatively cooled hydrogen arcjet system capable of operation in excess of 1000 s of specific impulse. Impressive results at the 30 kW power level were achieved as the Avco corporation demonstrated a 1010 s arcjet with an efficiency of 0.41 and a lifetime in excess of 700 h (ref. 2). The Giannini Scientific Corporation (GSC) also demonstrated a specific impulse of 1000 s at an efficiency of 0.55 and a 500 h lifetime (ref. 3) Lack of a suitable space power system resulted in the cancellation of the program, and little work was subsequently done on high power arcjets from the late 1960's to the mid 1980's.

The United States Air Force (USAF) has recently initiated electric propulsion efforts in support of an Electric Orbit Transfer Vehicle (EOTV) (ref. 4). Hydrogen arcjets were chosen for the EOTV, because of the relative maturity of the technology when compared to Magnetoplasmadynamic (MPD) thrusters. As a precursor to the EOTV, the Electric Insertion Transfer Experiment (ElITE) (ref. 5) is under development. This experiment, with a total of 10 kWe of solar power, will be used to demonstrate the feasibility of the EOTV for Earth-space orbit maneuvering using 10 kW ammonia arcjets for propulsion (ref. 5). To resolve the issues of lifetime and performance of the candidate thruster, a lifetest is underway at the Jet Propulsion Laboratory (JPL). A status paper indicated the thruster had completed 1136 h of the 1500 h test, with no significant problems (ref. 6). In addition to these programs, the Advanced Technology Transition Demonstration (ATTD) effort sponsored by the Phillips Laboratory

(PL) is developing a 26 kW ammonia arcjet system (ref. 4). Breadboard power electronics were developed in support of this effort and have been successfully integrated to an arcjet thruster (ref. 7). At the National Aeronautics and Space Administration's Lewis Research Center (NASA Lewis), a jointly sponsored program by the Strategic Defense Initiative Organization's Office of Innovative Science and Technology (SDIO/IST) and NASA's Office of Aeronautics and Space Technology (OAST) initiated hydrogen arcjet research, and obtained performance data between 5 and 30 kW using laboratory 60 Hz power supplies (ref. 8). In addition, 1 to 4 kW hydrogen arcjet performance was recently documented (ref. 9) using flight-like power electronics, hereafter referred to as power processing units (PPUs) (refs. 10 and 11). These lower power PPUs were developed in support of the hydrazine arcjet research effort which led to the development of a 1.8 kW auxiliary propulsion system for stationkeeping applications (ref. 12).

In support of these programs and the development of a 10 kW hydrogen arcjet system, a flight-like PPU was developed and integrated with an arcjet thruster. A power conversion efficiency of 0.93 and a packaged specific mass of 2 kg/kW were selected as design criteria to minimize the impact of the PPU on the overall system efficiency, spacecraft thermal control system, and overall mass. Input bus characteristics and arcjet impedance data were considered, and an input voltage of 150 V was selected. Impedance data taken from recent arcjet operations at 10 kW indicated arc voltages of 130 V or greater were likely (ref. 8), and that a high impedance PPU output characteristic was necessary for stable operation due to the negative slope impedance characteristic of the arcjet (ref. 10). A full bridge converter topology utilizing hybrid power Metal Oxide Semiconductor Field Effect Transistors (MOSFETs) and a low inductance layout were selected because of past successes with these designs at lower power levels (refs. 11 and 13). This paper documents the development, design, and operating characteristics of the 10 kW hydrogen arcjet PPU.

SYSTEM INTERFACES

Arcjet/PPU Interface

The arcjet geometry selected for use with this power processor incorporated a nozzle configuration described by Haag in high power hydrogen arcjet performance characterizations and is illustrated in figure 1. This anode geometry was listed as configuration B in reference 8 and the overall construction details of the arcjet were as described therein. The constrictor diameter and length were 1.8 and 3.6 mm, respectively, and the arc gap was set by inserting the cathode into the thruster until contact with the anode was made, and withdrawing it 0.9 mm. Volt-amp characteristics for configuration B appear in figure 2, but it must be noted that those data were taken with an arc gap of 1.27 mm (ref. 8). The data show a negative slope volt-amp characteristic typical of arcjets. Due to facility constraints in this study, the mass flow rate was limited to 45.8 mg/s, which resulted in a maximum expected arc voltage of approximately 135 V at 50 A arc current. From those data, it was decided to set the maximum output voltage of the PPU at 225 V to allow for contingencies and possible geometric changes of the electrodes. The maximum output current was also set at 100 A to allow for 10 kW operation at arc voltages as low as 100 V if necessary. A steady state output ripple of 15 percent was specified based on previous designs (refs. 10, 11, and 13), and indications that lower ripple magnitudes accelerate erosion of the arcjet electrodes (ref. 14).

In previously developed PPUs arcjet ignition was accomplished using a high voltage pulse (refs. 7 and 10 to 13). This technique was chosen for this design because of the wide application base and the inherent capability to tailor pulse parameters such as amplitude, duration, and energy content.

Spacecraft/PPU Interface

Input voltages in excess of 150 V would result in lower input currents at 10 kW, but these higher voltages could result in other complications such as environmental interactions and were not considered here. It was also assumed that a 28 V low power bus would be present, and all control power would be derived from this low voltage bus. The unit described in this paper derived control power from 110 Vac mains, but a design for a 28 V input control power converter is included in the appendix. The issues of overall system efficiency and waste heat at this power level were important from a mission standpoint, therefore, a power conversion efficiency of 0.93 was considered the minimum acceptable, resulting in a spacecraft heat load of 700 W. This work focused on the development of the power converter and did not address packaging or electromagnetic compatibility issues.

DESIGN

Power Topology

An isolated, single phase topology which electrically isolated the load from the input bus was selected for this work. Isolated topologies have several advantages when compared to nonisolated designs, but both have been successfully applied to arcjets in the laboratory environment. The key advantages of the isolated design were the ability to conform to single point grounding systems, and the ability to operate in the boost or buck mode. It should be noted however that the boost or buck regulators tend to be less massive than the isolated topologies because of the simpler magnetic circuits used. For example, the 30 kW three phase buck regulated PPU developed by Wong et al. for ammonia arcjets, demonstrated an efficiency on the order of 0.95 with a specific mass of 1.8 kg/kW for the breadboard (ref. 7). A single-phase design was chosen for this PPU because it was decided that the power level did not warrant the added complexity of additional phases in parallel or in a staggered-phase configuration. A full bridge configuration, illustrated in figure 3 was selected for the power stage. This power stage has been applied to arcjet PPUs in the past, and the details of its operation were described elsewhere (refs. 11 and 13). Briefly, switches $\Phi 1$ and $\Phi 2$ were operated at a 50 percent duty cycle and were referred to as the reference phase. Switches $\Phi 3$ and $\Phi 4$ were also operated at a 50 percent duty cycle and were in phase with the reference side for a zero output. The duty cycle of the converter was increased by shifting the phase angle of $\Phi 3$ and $\Phi 4$ with respect to the reference side. Full output was realized when the phase angle reached 180°. Variation of the duty cycle and thus the output voltage as the load varied, maintained a constant output current.

A block diagram of the PPU appears in figure 4, and an overall schematic is shown in figure 5. Each component of the PPU is discussed in the following sections.

Controls

A pulse width modulated (PWM) current mode control scheme similar to that used by Gruber in previous efforts was used in this design and has been described in detail elsewhere (refs. 10 and 11). A block diagram of this PWM controller appears in figure 6 and a schematic is shown in figure 7. This controller was designed to operate with a push-pull power stage, a topology which employs only two switching transistors. Some additional circuitry was required to convert the output of the PWM controller to operate the four transistor, phase shifted bridge power stage. The phase shift converter circuit was described in detail elsewhere (ref. 13), and a schematic of the phase shift circuitry appears in figure 8.

A modification developed by Gruber for the 5 kW power electronics, but not reported in reference 10, was the addition of a soft-starting circuit to limit the initial arc current at breakdown. This circuit utilizes the inherent cycle-by-cycle current limiting capability of the PWM controller, which is a fault protection scheme, to override the error signal from the integrator. Saturation of the integrator caused by the absence of output current during the interval between PPU power up and arc ignition caused the PPU to phase up to 100 percent output, resulting in high arc currents at breakdown until the integrator ramped down to the proper level. This, coupled with the normal low voltage mode ignition of the arc, could cause severe anode damage. The circuitry which accomplished this is outlined in a dashed box in figure 7. The operational current limit of the PPU was set by the voltage divider on pin 1 of the current mode controller. A series Resistor-Capacitor (RC) network was added to pin 1, and a FET was connected in parallel with the capacitor as shown. When the pulse ignition circuit was charging, the capacitor was shorted by the FET, placing the series resistance of the RC network in parallel with the current limit voltage divider, reducing the current limit. When a pulse was generated and the arcjet ignited, the FET was turned off, allowing the capacitor to charge back up and the original current limit reference returned to pin 1. The ramp up time was controlled by the size of the components in the series RC network and voltage divider.

Power Stage

Power MOSFET switches were selected because of their superior performance at the 150 V input when compared to Insulated Gate Bipolar transistors (IGBT)s or MOS Controlled Thyristor (MCT) devices. At this voltage level, the MOSFETs have lower conduction losses and faster switching speeds. Because operation of the PPU at duty cycles of 50 percent at 10 kW was possible, the switches would have to safely handle peak currents on the order of 150 A. This could have been accomplished by paralleling many individually packaged transistors, but would have involved much weight, space, and the potential for high inductances in the device interconnections. Instead, a hybrid power FET was used. A 200 V, 360 A package was selected, and other data for this device appear in table I (ref. 15) The selection of 200 V devices with a 150 V input bus at 10 kW required special attention to power stage parasitic inductances in order to minimize switching transients, and the associated power dissipation in the snubbers, or damping circuits used to control them. Loop areas were minimized in the interconnections between the input bus, power transistors, and the transformer. The end result was the power stage assembly shown in figure 9. The positive and negative input busses were formed into plates which covered the upper surface of the FET packages, and interlocked as shown. The drain-source-transformer connections on either side of the bridge were made with plates sandwiched between the input power bus plates. All conductors were coated with insulating tape, except where electrical connections were necessary, and held together with nylon screws.

Gate Drive

The phase shifted bridge topology posed a problem with the gate drives in that the source terminals of each FET were not all connected to the same point. This required gate drives with a different reference ground for each FET, although the bottom two FETs in the bridge do share a common source connection. High speed isolated gate drives were developed by Stuart et al. (ref. 16) for this purpose and used in a previous lower power design (ref. 13). These gate drive circuits employed an integrated circuit driver, which though quite adequate for driving a small number of paralleled FETs, could not sufficiently drive the power hybrids. To compensate for this, a totem pole output was added to the circuit. A complete schematic of the gate drive circuit appears in figure 10.

Power Transformer

A tape wound, cut "C" Nickel-Molybdenum-Iron core with a tape thickness of 0.025 mm was used as the basis for the power transformer. The cross sectional area of the core was 6.45 cm^2, with a stacking factor of 0.85. The first design employed 11 turns in the primary winding to reduce the flux density in the core, however, it was found that the leakage inductance associated with this design was greater than 2 μH. The snubbers required to dissipate the energy in this leakage inductance were large, and represented a power loss greater than the core losses saved by the additional turns. The final design, incorporating six turns in the primary utilized the maximum allowable flux density in the core. This resulted in a leakage inductance of less than 1.5 μH. An air gap of 0.04 mm was added to eliminate flux imbalances during operation. The primary and secondary were wound with 2 AWG Litz wire, and the turns ratio was 6:8. A cutaway view of the power transformer appears in figure 11.

Output Filter and Start Circuit

The desired output current ripple of about 15 percent resulted in a calculated value of 125 μH for the output inductor. A gapped, tape wound, cut "C" core construction was chosen to minimize size and weight. The core tape material was grain oriented silicon steel with a tape thickness of 0.025 mm. The cross-sectional area of the core was 6.45 cm^2. Construction details of this inductor were similar to the transformer design illustrated in figure 11. Twenty turns of number 4 AWG square magnet wire were wound on the core and the gap set to 2.54 mm for an inductance of 125 μH. The output filter inductor was also used as a pulse transformer during startup of the arcjet. This pulse ignition technique used has been described in detail elsewhere (ref. 17) and has been used in other isolated topology PPU designs (refs. 10, 11, and 13). A schematic of the start circuit is shown in figure 12. An additional five-turn winding was added to the output inductor which acted as the primary for the pulse transformer. This winding was charged by turning on FET Q1 in figure 12, thereby discharging the 33 000 μH electrolytic capacitor through the winding. The "on" time was on the order of 50 μs. FET Q1 was then turned off, and the resulting large negative di/dt in the primary generated a high voltage pulse across it. The high voltage pulse was then amplified through the turns ratio of the output inductor. The amplitude and duration of the start pulse were controlled by tuning the RC snubber and Diode-Resistor-Capacitor (DRC) clamp across Ql. In previous designs, a 1:10 turns ratio was used, but in this case, the small number of turns on the output inductor made this impractical. Also, the small filter inductance limited the energy storage capacity. A 1:4 turns ratio was used as a compromise between voltage gain and reasonable primary inductance. The inductance of the pulse winding was 9.3 μH.

Initially, when the PPU was operating, there was a significant ac voltage component on the output inductor, and this ac component was transferred to the pulse winding by transformer action. This ac component resulted in power dissipation in the snubber and clamp resistors, and significant heating resulted. To eliminate this power loss, FET Q2 in figure 12 was added to remove the current path to these devices when the pulser was not in operation. This FET was normally in an "on" state, until arc current was sensed. It was then shut off to isolate the snubber and clamp circuits.

PERFORMANCE

Physical Characteristics

The PPU was constructed on a fiberglass sheet 61 by 61 by 1.27 cm. A photograph of the completed unit is shown in figure 13. Cooling was accomplished using heatsinks and small fans. The total

mass of the entire breadboard was 29 kg, including the fiberglass baseplate. The component mass was 22.7 kg, but this mass also included 6 kg of nonflight rated parts such as 60 Hz magnetics, cooling fans, and the large electrolytic capacitors at the input. A mass of 16.7 kg resulted when these items were subtracted. The remaining 16.7 kg mass also included the heat sinks and mounting hardware used in the construction of the breadboard. From these data, a specific mass of 2.0 kg/kW for a flight packaged unit was projected.

Output Characteristics

The open circuit voltage of the PPU was measured at 225 V for a 150 V input. The lack of a suitable range of load resistance prevented the collection of data necessary to plot a volt ampere characteristic. Load regulation was measured to be less than 1 percent from 135 to 150 V input which was consistent with previous designs (refs. 10, 11, and 13) and the line regulation was of the same order. Output current ripple was 15 percent at 85 A output. The PPU was capable of stable operation at output voltages of less than 100 V and power levels as low as 1.5 kW into resistive loads. The maximum output power demonstrated was 11.5 kW and this was limited by the input power supply. Based on the conservative component selection and conductor sizes, operation at power levels as high as 13 kW would be possible with a suitable power source and cold plate cooling. The performance of the critical components of the PPU is discussed in the following sections.

Gate Drives

An oscillograph of the gate drive signals for the reference side of the bridge is shown in figure 14. The traces have been aligned in the figure so that their zero values were equal, and the transistors were on when the drive signal was 15 V. Note that a period of approximately 500 ns existed when both transistors were off. This prevented the simultaneous turn on of both transistors in one side of the bridge. The turn on and turn off times for the gates were on the order of 150 ns.

Power Stage

When the initial design of the power stage was implemented, it was hoped that snubberless operation would be possible. This notion proved to be overly optimistic. A series RC snubber was added in parallel with the transformer primary to suppress the turn on transient across the transformer primary. This type of snubber proved to be more effective than other types in parallel with the switches, and was also optimal in terms of dissipation. Oscillographs of the power transformer primary voltage and current waveforms with the snubber appear in figures 15(a) and (b). The load conditions were 120 V output at 83.3 A, and the input voltage was 145 V. The turn on spikes were clearly evident, but were less than the 200 V rating of the power MOSFETs. The transients were also well controlled at 150 V input. A di/dt loss was evident as a 10 V drop in the primary voltage immediately after turn on. This loss occurs during the large di/dt present when the primary current changed direction. Since the primary voltage was measured directly at the transformer, this voltage drop must have occurred in parasitic inductances in the switches and power stage interconnections. An inductance of 75 nH was calculated from these data. As the duty cycle of the converter increased with higher output voltages at a fixed power level, the magnitude of these transients decreased due to the lower peak input currents. Series RC snubbers were also added in parallel with the output rectifiers to suppress turn off transients.

Efficiency

The power conversion efficiency was measured using commercial shunts to measure PPU input and output currents with resistive loads. Digital voltmeters were used to measure the input and output voltage, and the shunt voltages. These measurements were done at NASA Lewis and the University of Toledo, using different voltmeters, but the same set of shunts. The efficiency was also measured at the University of Toledo using Hall effect current probes in conjunction with a digital oscilloscope. These measurements agreed with those taken with the digital multimeters within 0.5 percent. At NASA Lewis, the efficiency measured for a 2.75 Ω load at 10 kW was 0.947 for a 165 V output after 5 min of operation. Efficiencies at lower output voltages for the same power level decreased due to higher primary currents and increased output rectifier losses. At the University of Toledo, the efficiency measured for a 2.6 Ω load was 0.948 at 10 kW after 5 min of operation. The results of these efficiency measurements appear in figure 16. These data were taken by increasing the PPU output current into a fixed resistive load. Approximately 2 min elapsed between each data point. After 30 min of operation at 10 kW, with the PPU in thermal equilibrium the efficiency was found to drop approximately 0.007 . This loss in efficiency resulted from increased conduction losses due to inadequate cooling.

The transformer design proved to be extremely lossy. After 30 min of operation, the core temperature exceeded 65 °C. It should be noted that the transformer was in still air, and no active cooling measures were applied. Losses in the transformer could be reduced by increasing the number of turns on the primary winding, reducing the induction level. The eddy current losses in the core could also be reduced if a 12.7 mm wide tape were used instead of the 24.5 mm wide tape. Core losses in the present design were estimated in excess of 160 W. From these data, the steady state efficiency of the PPU was projected as 0.94 with load voltages in excess of 150 V. This efficiency could be improved by as much as 0.5 percent with transformer redesign and adequate cooling.

ARCJET INTEGRATION TESTING

The PPU was integrated with the arcjet described earlier and tested in the Tank 5 Space Environment Facility at NASA Lewis. The goal of the initial testing was to verify the capability of the PPU to successfully start the arcjet. An oscillograph of open circuit start pulse used appears in figure 17. The amplitude of the start pulse was 2.1 kV with a duration of 8.5 μs. During initial testing an arcjet similar in configuration to that in figure 1 was used, with the exception of the gap length, which was 2.5 mm. The flow rate used was 45.8 mg/s. In these tests, the pulse of figure 17 would not break down the gas between the electrodes. The flow was reduced to one fourth of the initial value and breakdown into a glow discharge occurred. The glow discharge breakdown voltage was on the order of 600 V. At this voltage, the PPU was unable to supply energy to sustain the discharge, and it extinguished when the output inductor ran out of energy. The peak charging current on the pulse transformer primary was 250 A, corresponding to 290 mJ of stored energy.

The arc gap was then reduced to 0.9 mm, and the tests repeated. Arc ignition was not a problem with this arc gap for the full operational flow rate. A typical start was shown in figure 18. At the initial breakdown, an 80 A, 2 μs spike occurred as the capacitance in the output cables and PPU output discharged. Following this spike, the initial arc current was limited to the preset 35 A starting current limit. During this start the arc current operating reference was also set to 35 A. The arc current ramped upward to 80 A, until the integrator error signal ramped the arc current down to the 35 A setpoint. The initial arc discharge voltage was 26 V, increasing to 63 V. This low voltage mode operation lasted approximately 30 ms. The current overshoot occurred while the thruster was in the low voltage mode, but no anode damage was evident. Adjustments of the time constant of the soft start circuit would

reduce this current overshoot, but because the peak overshoot current did not exceed the arc current expected at 10 kW, none were made. After 33 ms the arc voltage increased to approximately 120 V, the nominal operating voltage. The arc voltage and current for a 10 kW operating point are shown in figure 19. Of interest here is the voltage waveform. Typically in low power hydrazine arcjets, the arc voltage waveform appears identical to the current waveform with a 180° phase shift (ref. 18). In this case, it appears that the voltage signal is distorted by the inductance of the thruster and power cables. The effect of thruster and cable inductance may be exaggerated when comparing waveforms with lower power thrusters because of the larger magnitude of the current ripple present here.

CONCLUSIONS

In support of Earth-space orbit transfer and maneuvering propulsion programs, a flight-like 10 kW PPU for hydrogen arcjets was fabricated and integrated with a laboratory arcjet thruster. Thruster volt-ampere data taken during preliminary performance tests with laboratory power supplies were used to determine the output characteristics of the PPU. A maximum output voltage of 225 V was selected based on these data and the output current ripple magnitude limited to 15 percent. Conductors and components were sized to allow operation at arc currents as high as 100 A. A full bridge topology was selected for the power stage which provided line/load isolation. Power hybrid MOSFETs in conjunction with high speed optically isolated gate drives were used to minimize conduction and switching losses, and a low inductance layout was developed to limit transients and minimize snubbing requirements. The breadboard power electronics demonstrated an efficiency of 0.94 and a packaged specific mass on the order of 2 kg/kW was projected. Starting techniques identical to those used in previous efforts were used and successfully started the arcjet. Transitions from initial breakdown to steady state were uneventful.

ACKNOWLEDGMENTS

The authors would like to acknowledge Dr. Thomas Stuart and Dr. Roger King for their technical support and the use of the power electronics laboratory at the University of Toledo for the efficiency measurements. Also, Dr. Duane Rost at Youngstown State University is acknowledged for technical guidance.

APPENDIX

A 28 V input power converter was built to supply control and gate drive power to the 10 kW unit. A flyback configuration, as shown in figure Al, was selected due to its simplicity. In this topology, when the switch was turned on, an increasing flux was induced in the transformer core. There was no current flow in the secondaries because the diodes were reverse biased. When the switch was turned off, the transformer primary reversed polarity and the energy stored in its core induced a current in the secondaries through the forward biased diodes.

A molybdenum permalloy powder (MPP) core with a cross sectional area of 0.654 cm^2 was used for the power transformer. A clamp across the primary winding and an RC snubber on the MOSFET were used to reduce transients and ringing. An 18:10 turns ratio was used on the five secondary windings. Two windings with the same reference were used to produce 15 and -15 V for the PPU controls and the gate drive power for Q2 and Q4 of figure 3. Two other windings produced 15 V for the gate drives Q1 and Q3 of figure 3, respectively. The remaining winding was a sense winding that generated the feedback signal for the control circuit.

A 20 kHz pulse width modulated current mode control circuit, similar to that used in the 10 kW unit, but without the pulser circuitry, was used in this converter and was illustrated in figure A2. The output of the converter can be controlled by a potentiometer that varied the reference signal in the error integrator of the control circuit. Because only one MOSFET was used in the power stage, the output of the UC1846 provided sufficient gate drive.

REFERENCES

1. Sankovic, J.M., et al.: Hydrogen Arcjet Technology. NASA TM-105340, 1991.

2. John, R.R.: Thirty-Kilowatt Plasmajet Rocket Engine Development. Summary Report on the Second Year Development Program. NASA CR-54044, 1964.

3. Todd, J.P.: 30 kW Arc-Jet Thrustor Research. Giannini Scientific Corporation, APL-TDR-64-58, Mar. 1964.

4. Sanks, T.M.; Raygor, B.L.; and Birkan, M.A.: The Status And Future Plans For Electric Propulsion Development By The United States Air Force. IEPC 91-006, Oct. 1991.

5. Vondra, R.: Electric Insertion Transfer System (ELITE)—Mission Profile and Architecture Trades. Presented at the JANNAF Conference, Feb. 1992.

6. Polk, J.E.; and Goodfellow, K.D.: Endurance Test of an Ammonia Arcjet at 10 kWe. IEPC 91-068, Oct. 1991.

7. Wong, S., et al.: Operational Testing of the Power Conditioning Unit for a 30 kWe Arcjet. Proceedings of the Eighth Symposium on Space Nuclear Power Systems, M.S. El-Genk and M.D. Hoover, eds., American Institute of Physics, New York, 1991, pp. 982-987.

8. Haag, T.W.; and Curran, F.M.: High Power Hydrogen Arcjet Performance. AIAA Paper 91-2226, 1991 (also, NASA TM-105143, 1991).

9. Curran, F.M., et. al.: Medium Power Hydrogen Arcjet Performance. AIAA Paper 91-2227, 1991.

10. Gruber, R.P.: Power Electronics for a 1 kW Arcjet Thruster. AIAA Paper 86-1507, 1986 (also, NASA TM-87340, 1986).

11. Gruber, R.P.; Gott, R.W.; and Haag, T.W.: 5-kW Arcjet Power Electronics. AIAA Paper 89-2725, 1989 (also, NASA TM-102108, 1989).

12. Smith, R.D., et al.: Development and Demonstration of a 1.8 kW Hydrazine Arcjet Thruster. AIAA Paper 90-2547, 1990.

13. Hamley, J.A.; and Hill, G.M.: Power Electronics for Low Power Arcjets. AIAA Paper 91-1991 (also, NASA TM-104459, 1991).

14. Harris, W., et al.: Effect of Current Ripple on Cathode Erosion of 30 kWe Class Arcjets. AIAA Paper 91-2455, 1991.

15. Gentron Powertherm Isolated Power Modules. Genton Corp., Scottsdale, AZ, 1990, pp. 2-205 - 2-215.

16. Stuart, T.A.; King, R.J.; and Chen, K.: An Investigation of Full Bridge DC/DC Converters for Arcjet Thrusters. NASA CR-187046, 1990.

17. Sarmiento, C.J.; and Gruber, R.P.: Low Power Arcjet Pulse Ignition. AIAA Paper 87-1951, 1987 (also, NASA TM-100123, 1987).

18. Hamley, J.A.: Arcjet Load Characteristics. AIAA Paper 90-2579, 1990 (also, NASA TM-103190, 1990).

TABLE I.—POWER MOSFET DATA (ref. 15)

V_{DSS}, V	200
I_D, A	360 at 25 °C
	144 at 100 °C
P_D, W	960
$R_{DS(on)}$, Q	0.004
Q_{GS}, μC	2.88
Weight, kg	0.4

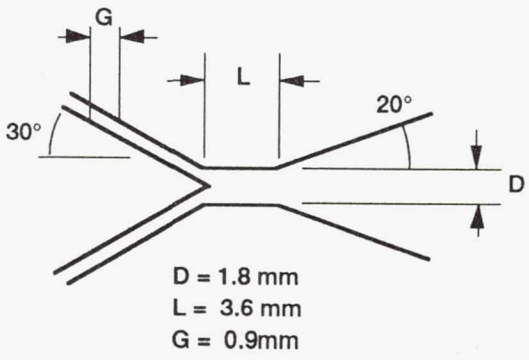

Figure 1.—Arcjet electrode geometry.

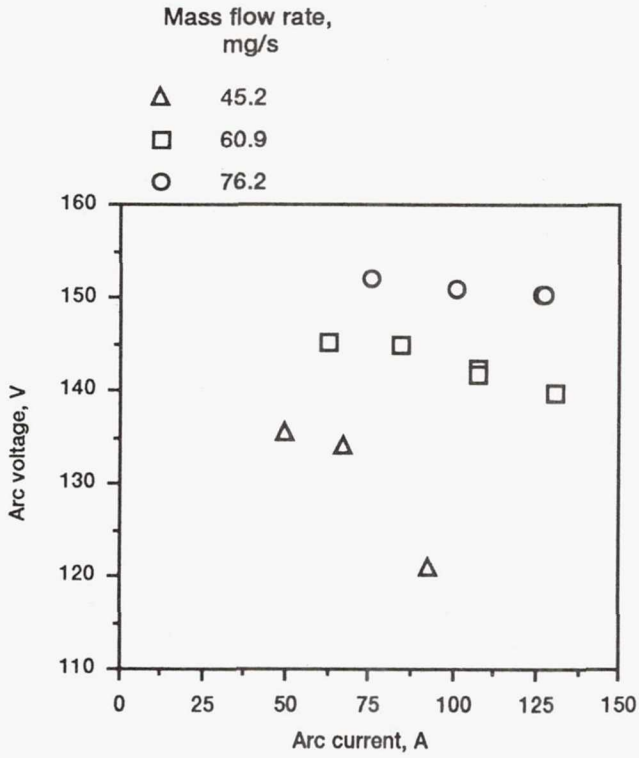

Figure 2.—Hydrogen arcjet volt-amp characteristics. (Reference 8.)

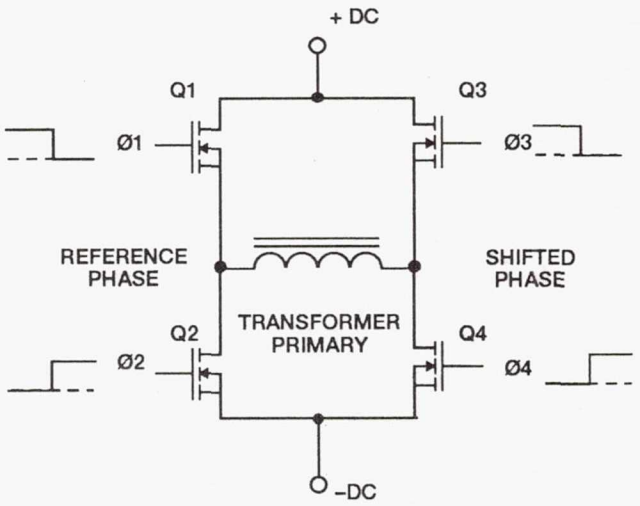

Figure 3.—Full bridge converter topology with phase shifted control. Gate drive signal Ø1-Ø4 are shown for zero output condition.

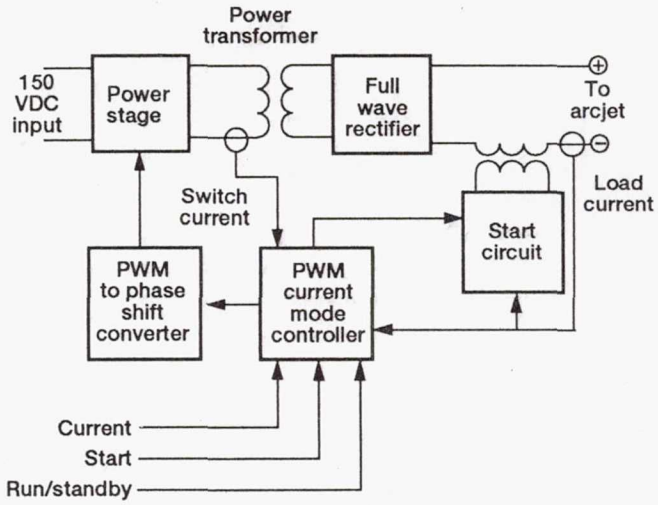

Figure 4.—10 kW hydrogen arcjet PPU block diagram.

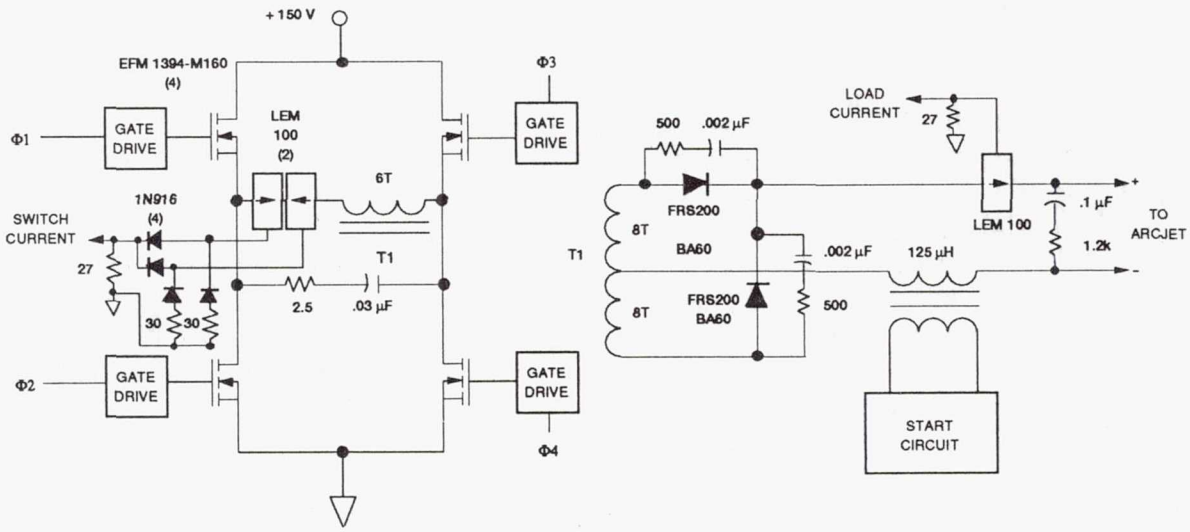

Figure 5.—10 kW hydrogen arcjet PPU schematic.

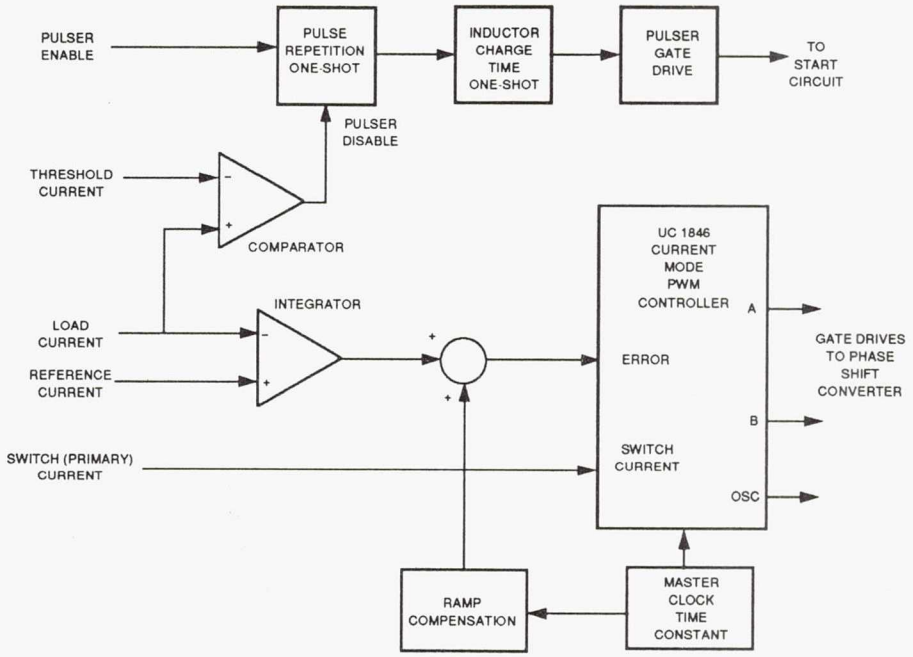

Figure 6.—PWM controller block diagram.

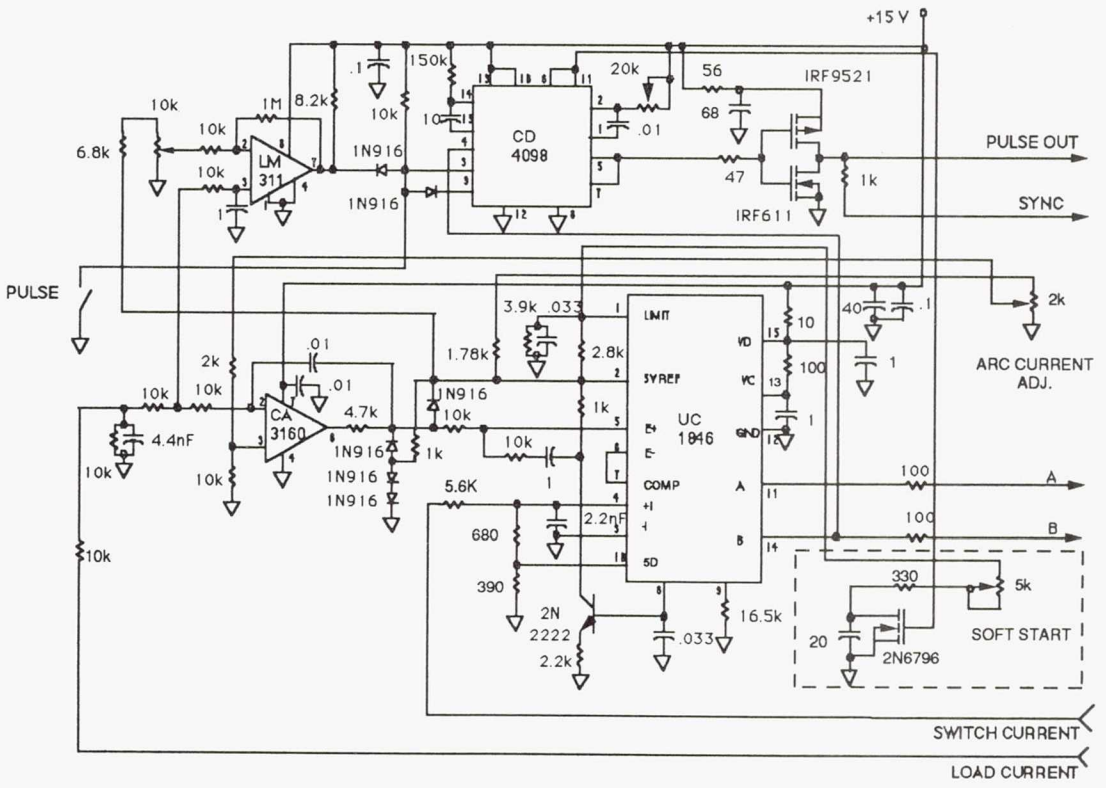

Figure 7.—PWM controller schematic (Reference 10) modified for 10 kW operation. All resistances are in ohms, and capacitances in microfarads unless otherwise noted.

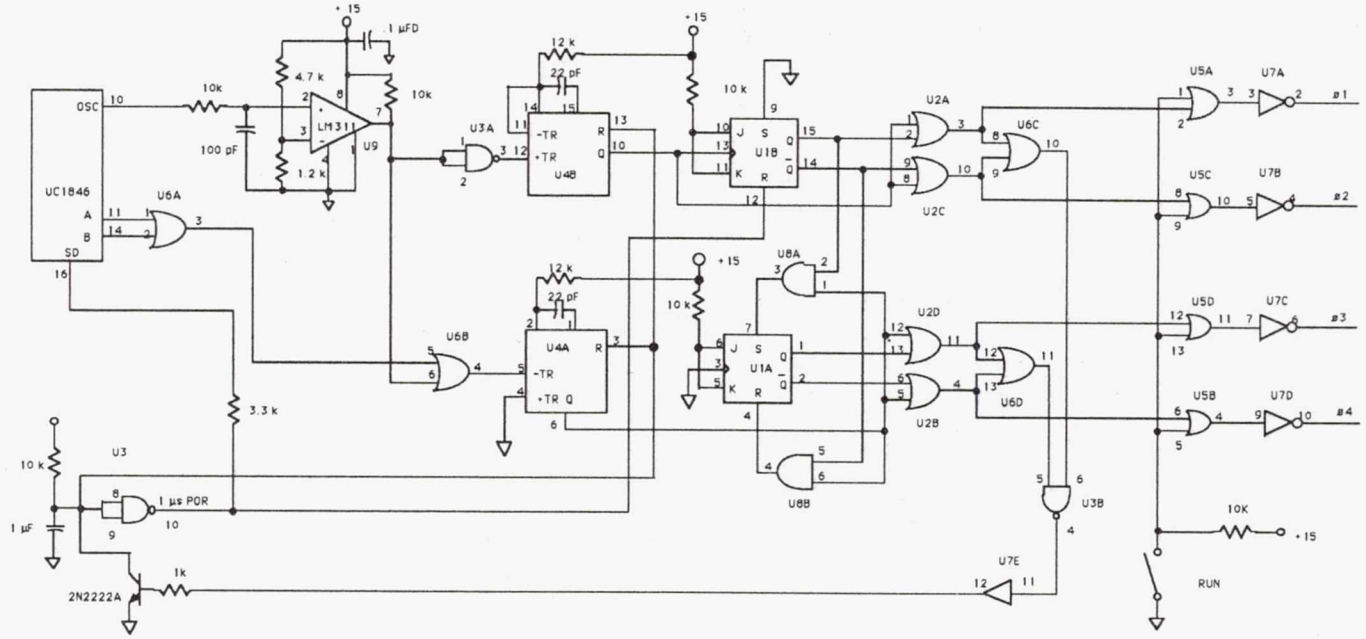

Figure 8.—PWM to phase shift converter circuit schematic (Reference 13).

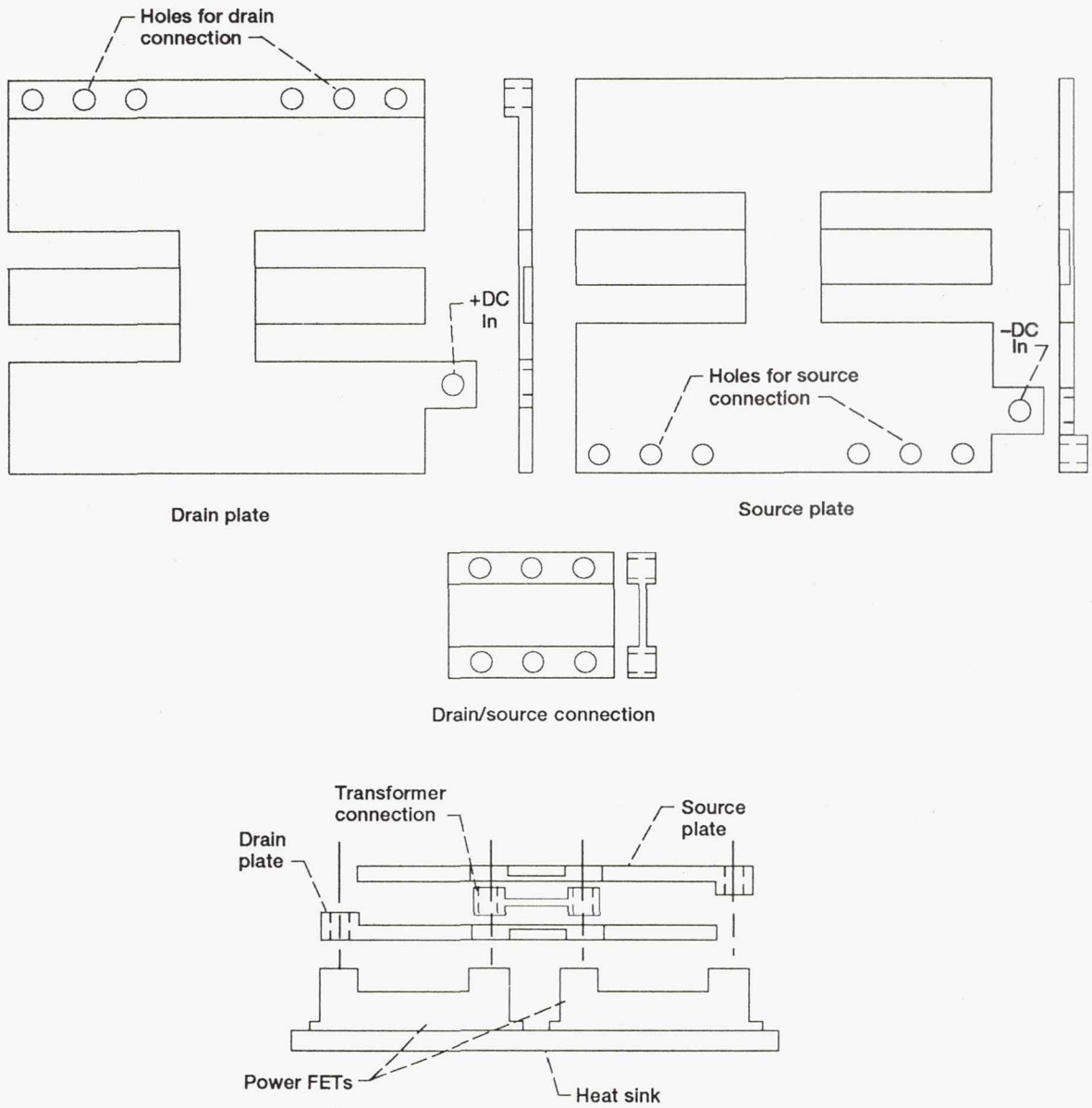

Figure 9.—Low inductance power stage assembly.

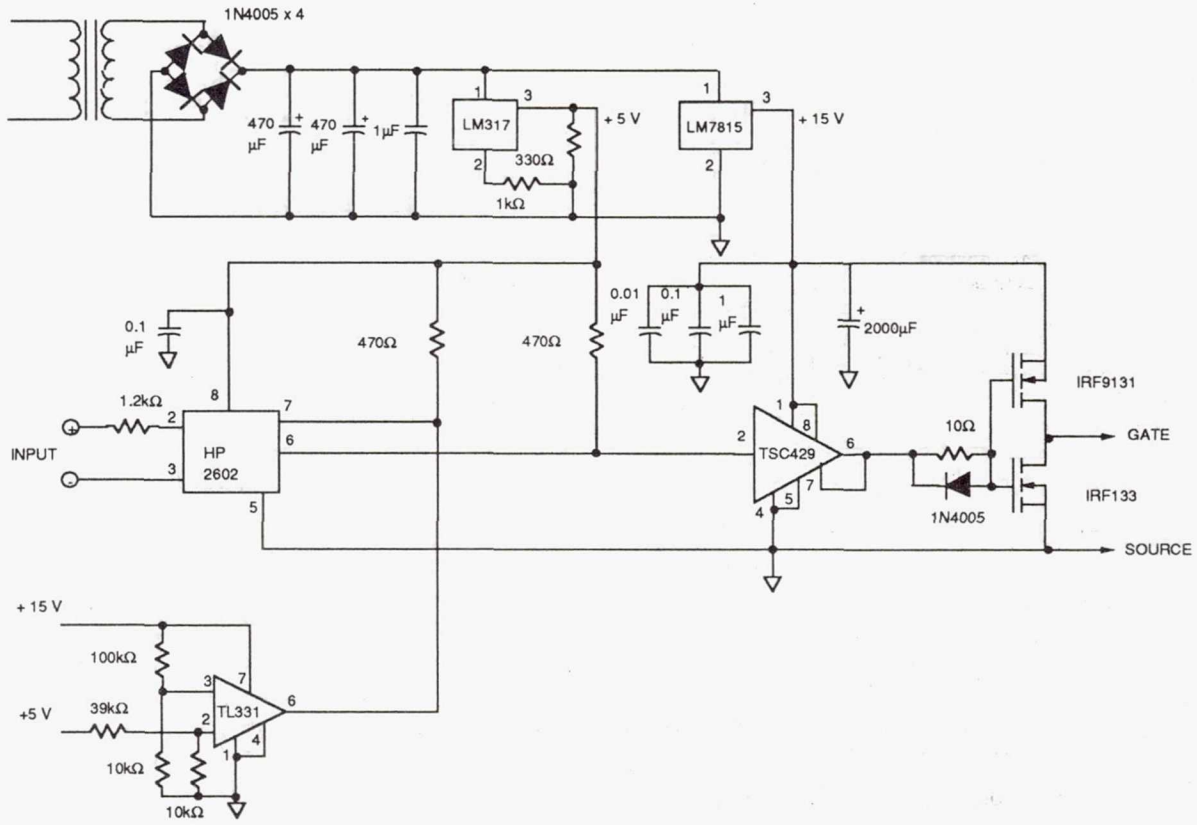

Figure 10.—Isolated gate drive circuit developed by Stuart et al. (Reference 16) with totem-pole output added.

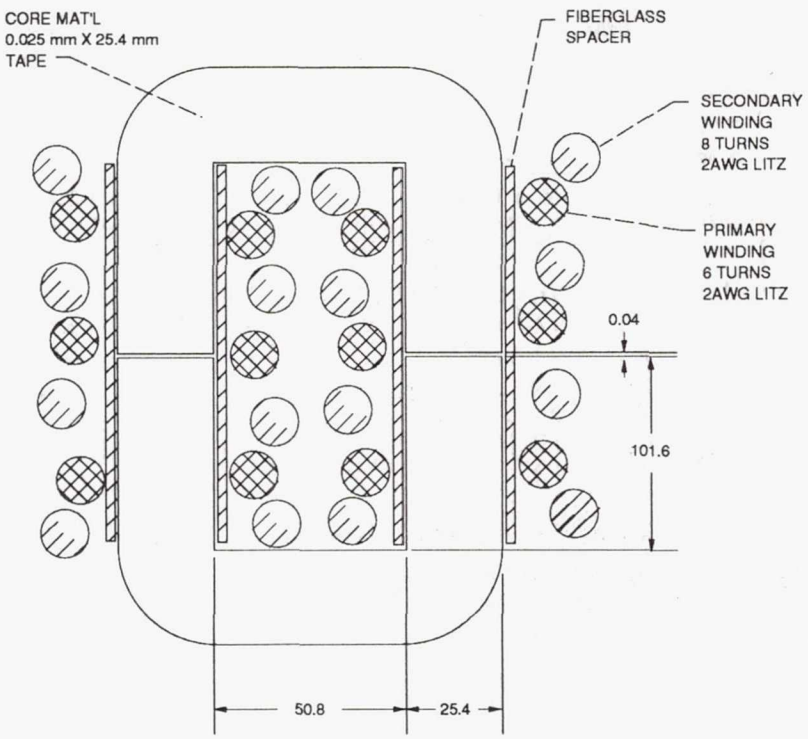

Figure 11.—Power transformer cross section. All dimensions are in millimeters.

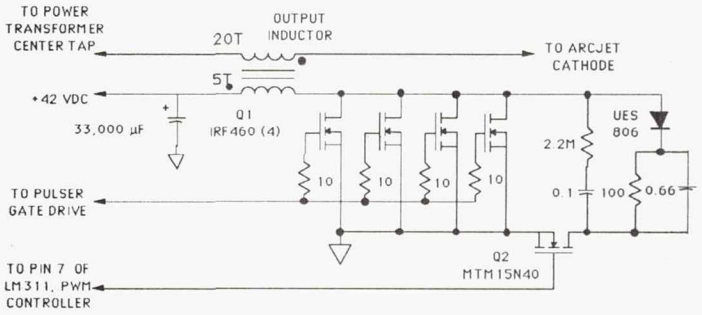

Figure 12.—Arcjet starter circuit schematic.

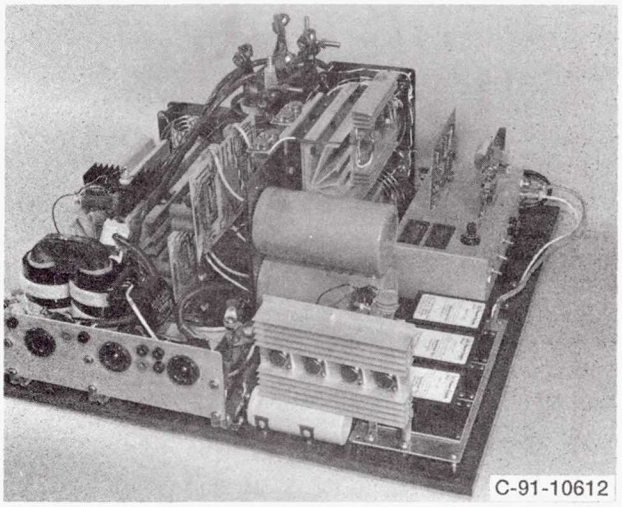

Figure 13.—Photograph of completed 10 kW PPU.

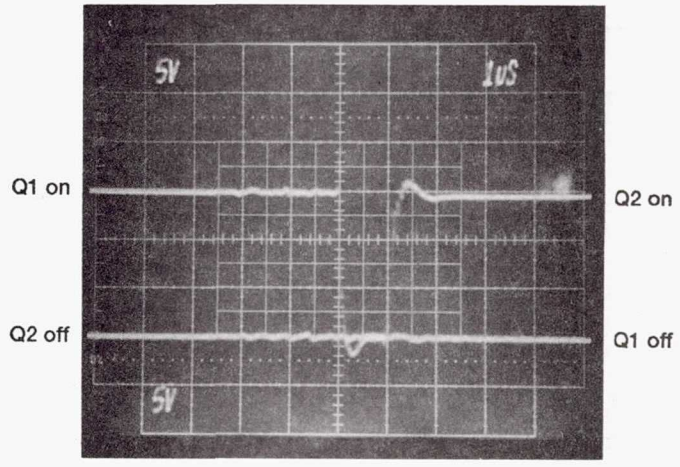

Figure 14.—Gate drives for transistors Q1 and Q2 of figure 3, illustrating turn off of Q1 and turn on of Q2.

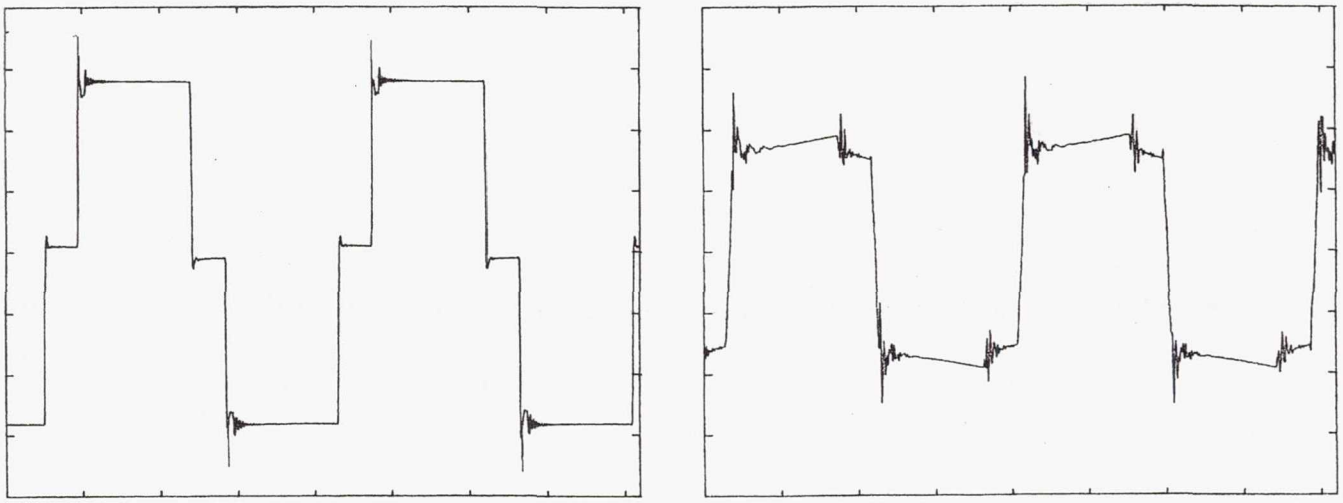

(a) Primary voltage: 50V/vertical division; 12.5 μs/horizontal division.

(b) Primary current: 50A/vertical division; 12.5 μs/horizontal division.

Figure 15.—Power transformer voltage and current waveforms for 10 kW output power.

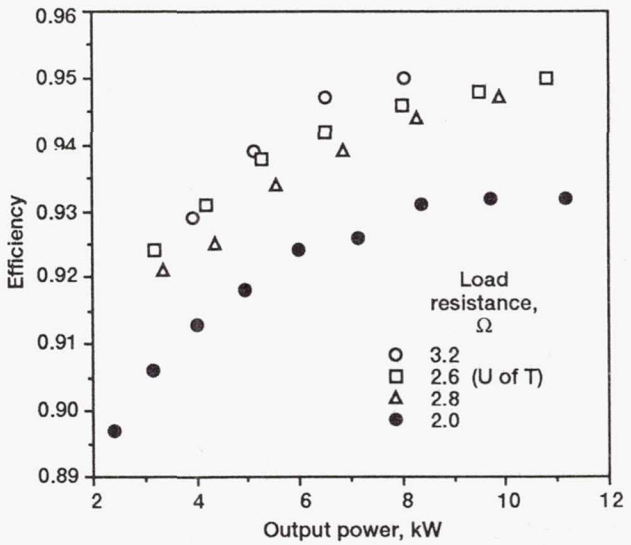

Figure 16.—PPU efficiency for various loads. Data from NASA and University of Toledo with two minutes elapsed time between each datum point.

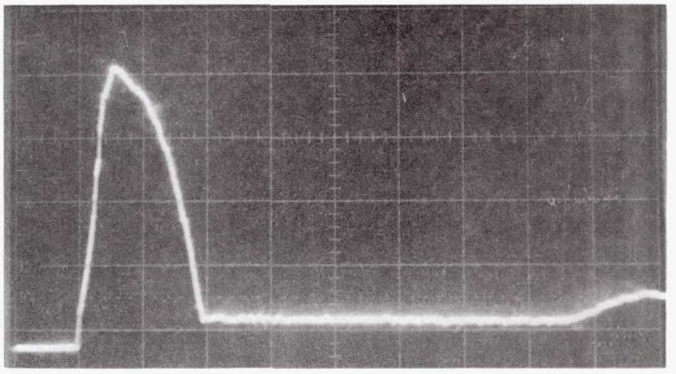

Figure 17.—High voltage start pulse at PPU output. 500V/vertical division. Time scale: 5 μs/horizontal division.

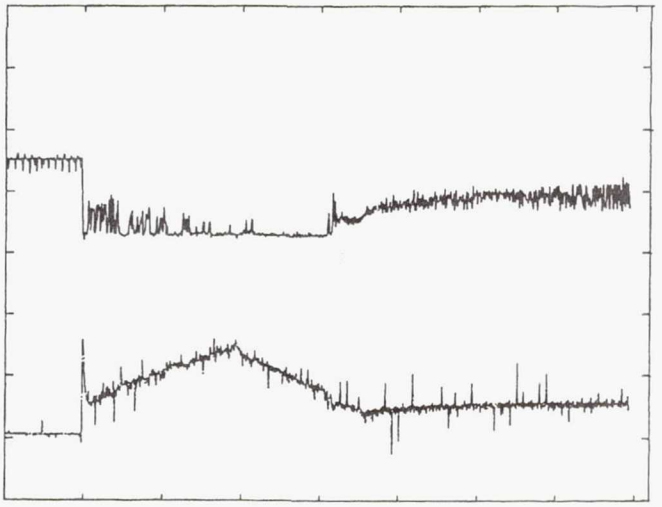

Figure 18.—Successful arc ignition. Upper trace: Arc voltage 125V/vertical division. Lower trace: Arc current, 50 A/vertical division. Time scale: 10 ms/horizontal division.

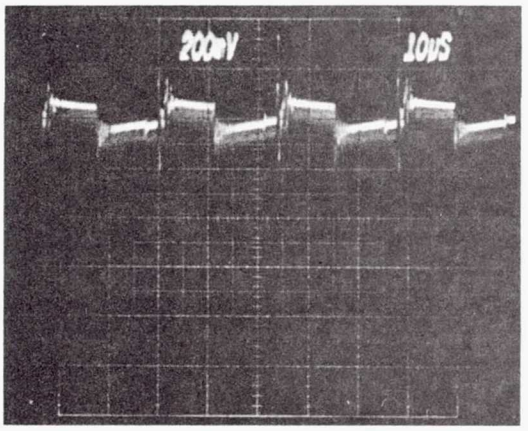

(a) Arc voltage: 20V/vertical division.

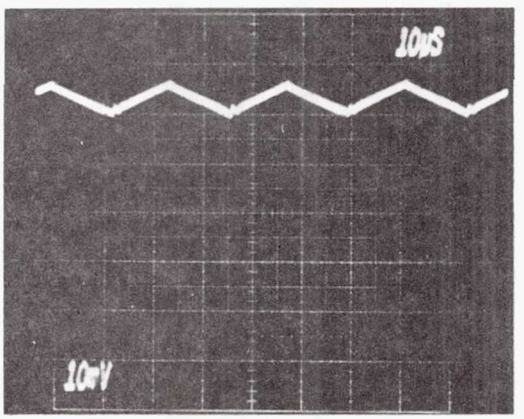

(b) Arc current: 20A/vertical division.

Figure 19.—Arc voltage and current waveforms at 10 kW arc power (120 V, 83.3 A).

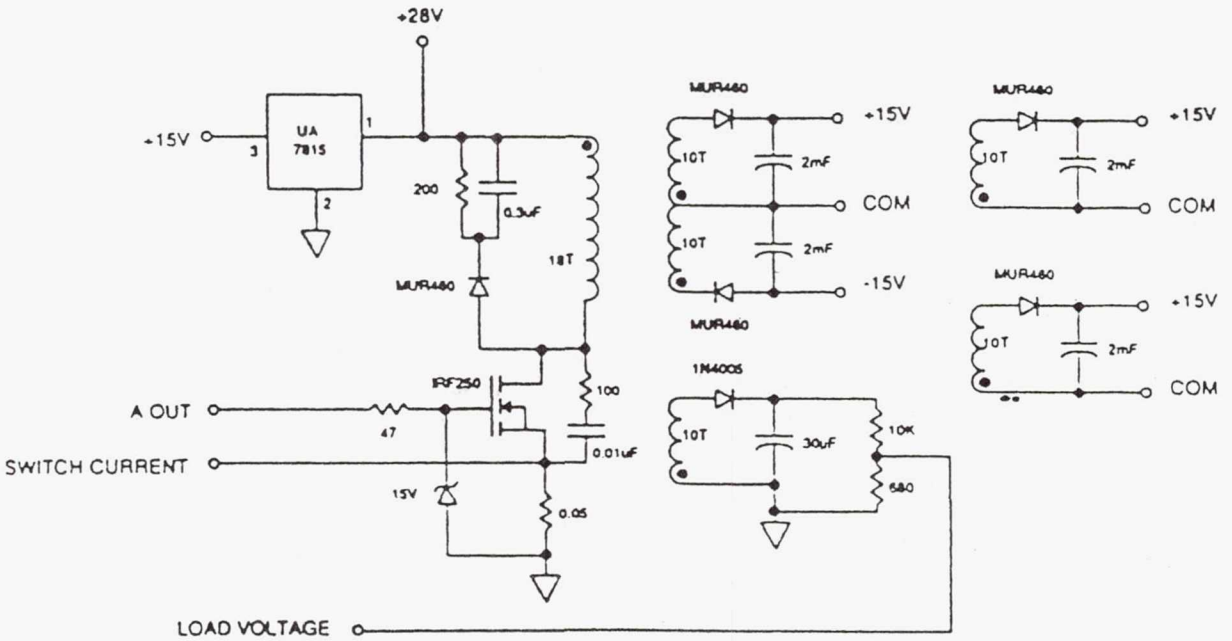

Figure A1.—Flyback converter schematic.

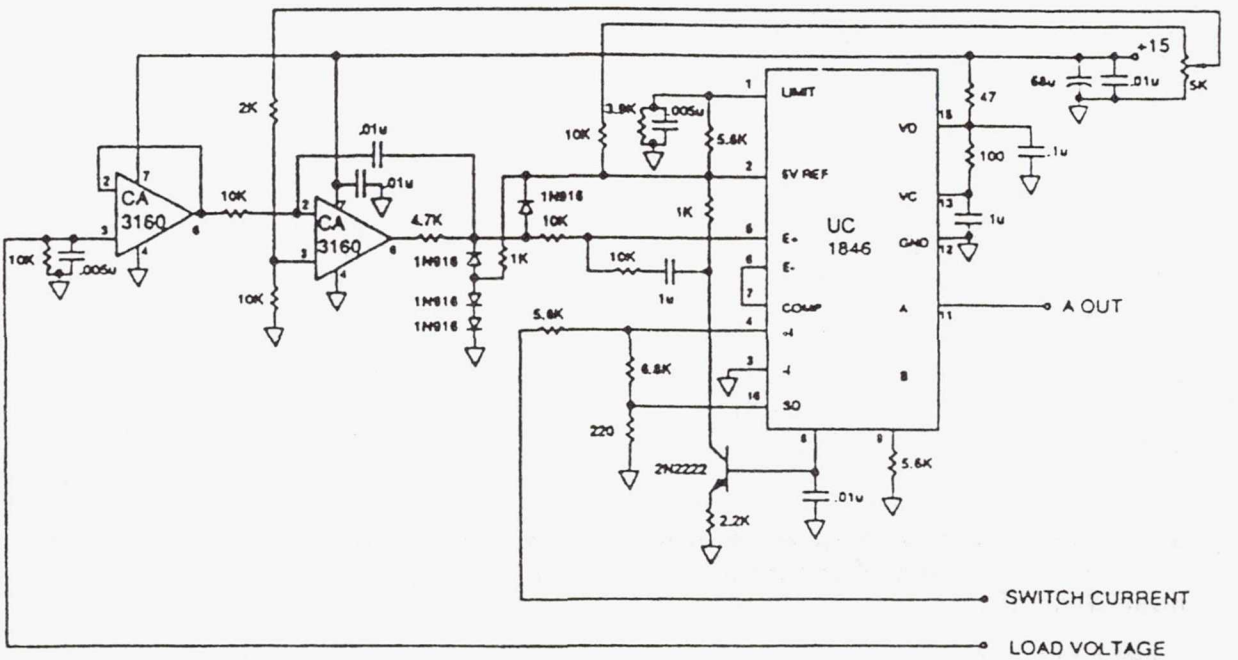

Figure A2.—Flyback converter controller.

REPORT DOCUMENTATION PAGE

Form Approved
OMB No. 0704-0188

1. AGENCY USE ONLY (*Leave blank*)	2. REPORT DATE	3. REPORT TYPE AND DATES COVERED
	1992	Technical Memorandum

4. TITLE AND SUBTITLE

10 kW Power Electronics for Hydrogen Arcjets

5. FUNDING NUMBERS

WU–506–42–31

6. AUTHOR(S)

John A. Hamley, Luis R. Pinero, and Gerald M. Hill

7. PERFORMING ORGANIZATION NAME(S) AND ADDRESS(ES)

National Aeronautics and Space Administration
Lewis Research Center
Cleveland, Ohio 44135–3191

8. PERFORMING ORGANIZATION REPORT NUMBER

E–6951

9. SPONSORING/MONITORING AGENCY NAMES(S) AND ADDRESS(ES)

National Aeronautics and Space Administration
Washington, D.C. 20546–0001

10. SPONSORING/MONITORING AGENCY REPORT NUMBER

NASA TM–105614

11. SUPPLEMENTARY NOTES

Prepared for the 1992 JANNAF Propulsion Meeting, Indianapolis, Indiana, February 24–28, 1992. Responsible person, John A. Hamley, (216) 977–7430.

12a. DISTRIBUTION/AVAILABILITY STATEMENT

Unclassified - Unlimited
Subject Category 20

12b. DISTRIBUTION CODE

13. ABSTRACT ***(Maximum 200 words)***

A combination of emerging mission considerations such as "launch on schedule," resource limitations, and the development of higher power spacecraft busses has resulted in renewed interest in high power hydrogen arcjet systems with specific impulses greater than 1000 s for Earth-space orbit transfer and maneuver applications. Solar electric propulsion systems with about 10 kW of power appear to offer payload benefits at acceptable trip times. This work outlines the design and development of 10 kW hydrogen arcjet power electronics and results of arcjet integration testing. The power electronics incorporated a full bridge switching topology similar to that employed in state of the art 5 kW power electronics, and the output filter included an output current averaging inductor with an integral pulse generation winding for arcjet ignition. Phase shifted, pulse width modulation with current mode control was used to regulate the current delivered to the arcjet, and a low inductance power stage minimized switching transients. Hybrid power Metal Oxide Semiconductor Field Effect Transistors were used to minimize conduction losses. Switching losses were minimized using a fast response, optically isolated, totem-pole gate drive circuit. The input bus voltage for the unit was 150 V, with a maximum output voltage of 225 V. The switching frequency of 20 kHz was a compromise between mass savings and higher efficiency. Power conversion efficiencies in excess of 0.94 were demonstrated, along with steady state load current regulation of 1 percent. The power electronics were successfully integrated with a 10 kW laboratory hydrogen arcjet, and reliable, nondestructive starts and transitions to steady state operation were demonstrated. The estimated specific mass for a flight packaged unit was 2 kg/kW.

14. SUBJECT TERMS	15. NUMBER OF PAGES
Arcjets; Hydrogen arcjets; Power electronics; Electric propulsion	22
	16. PRICE CODE A03

17. SECURITY CLASSIFICATION OF REPORT	18. SECURITY CLASSIFICATION OF THIS PAGE	19. SECURITY CLASSIFICATION OF ABSTRACT	20. LIMITATION OF ABSTRACT
Unclassified	Unclassified	Unclassified	